A Study of Algorithms for Detecting Pulsed Sinusoidal Interference in Microwave Radiometry

Joel T. Johnson and Lee C. Potter

***Abstract*— The performance of four algorithms for detecting the presence of pulsed sinusoidal interference in microwave radiometry is compared. The pulsed sinusoidal interference sources considered have unknown frequency, initial phase, amplitude, arrival time, and duration. Statistical properties of three of the algorithms are determined analytically, although numerical integrations are required in some cases in order to compute the obtained probabilities of detection. The performance of the fourth algorithm is evaluated using Monte Carlo procedures. Results show that three of the algorithms have a performance that is roughly comparable for the cases considered, while the fourth yields reduced sensitivity. A more detailed study of one of the algorithms, a simple energy detector called the pulse detection algorithm, is also provided.**

I. Introduction

Radio frequency interference (RFI) is a major concern for passive microwave remote sensing of the Earth's surface [1]-[2]. Traditional radiometer receiver architectures are very susceptible to RFI corruption of observed brightnesses; recent studies [3]-[11] are developing new radiometer technologies to address this issue. Combating the impact of RFI requires methods both for detecting the presence of RFI (detection algorithms) and for removing RFI when detected (mitigation algorithms.) This paper is focused on the problem of detecting that a particular radiometer observation contains RFI; methods for removing RFI are not considered.

While a variety of detection algorithms have been applied in radio astronomy applications (e.g. [12]-[14]), Earth remote sensing studies to date have primarily emphasized three particular approaches. The first two methods essentially involve a search for "outliers" in measured powers, based on either measurements as a function of time (i.e. a "pulse" detection method [4]-[5]) or frequency (i.e. a "narrowband" detection method [5]-[7].) Pulse detection strategies are designed to detect RFI with large amplitudes but short time durations (i.e. low duty cycle pulses), and are improved by matching the time resolution of the detector to the time duration of expected RFI pulses. Given the possible impact of long range air search radar systems on L-band radiometry, desirable time resolutions are often in the range of a few microseconds so that individual radar pulses can be resolved. Narrowband detection strategies are designed to detect frequency localized RFI that may be more continuous in time, and again are improved by matching the frequency resolution of the detection algorithm to the bandwidth of RFI sources.

Manuscript received Month dd, yyyy; revised Month dd, yyyy. J. T. Johnson is with The Ohio State University, Dept. of Electrical and Computer Engineering and ElectroScience Laboratory. L. C. Potter is with The Ohio State University, Dept. of Electrical and Computer Engineering

The third approach that has been utilized is based on a kurtosis algorithm [8]-[11]. In this technique, moments of observed fields up to the fourth order are computed by the radiometer system and used to compute the kurtosis (or fourth moment divided by the square of the second moment) of the observed field. Since observed fields should follow a Gaussian distribution in the absence of RFI, comparison of the measured kurtosis with the expected value for Gaussian fields provides an RFI detection algorithm that has been shown to be sensitive to the presence of pulsed interference [9] while retaining sensitivity to narrowband interference as well. The kurtosis algorithm can be applied directly to measured data or to individual subchannels created by an array of digital filters [8] or by an FFT operation. The latter approach is examined in detail in [14], and is termed the "spectral kurtosis" method in what follows.

A recent paper [9] has presented a derivation of the expected detection performance of the single channel kurtosis algorithm for pulsed sinusoidal interference. This paper performs a similar study for a simple power-based pulse detection algorithm and compares the results obtained with those achieved by the kurtosis and spectral kurtosis techniques.

The more general theory of detection problems [15] provides a framework for interpreting these results, as well as an additional detection algorithm for comparison. It is generally expected that the performance of a detector will improve as more information on properties of the interference are incorporated into the detector. The ideal case of perfectly known RFI in the presence of additive white Gaussian noise allows proof that a matched filter detector is the optimal approach. For RFI that is not completely known (as is the expected case in Earth remote sensing,) no uniformly most powerful detector exists [15]. Nevertheless, standard approaches have been developed that appear to provide very good results in practice.

One of these approaches is the generalized likelihood ratio test (GLRT), which is computed by using maximum likelihood estimates of unknown signal parameters in a likelihood ratio test of a known signal. An implementation of the GLRT is described in [15] for detecting the presence of pulsed sinusoidal interference of unknown frequency, amplitude, time of arrival, and initial phase. The resulting algorithm is based on "peak picking" a spectrogram comprised of short time Fourier transforms of the observed data. This paper compares results from the peak picking algorithm with those from the pulse, kurtosis, and spectral kurtosis methods. The results demonstrate the advantages of incorporating additional information on an RFI source: the kurtosis algorithm assumes only that the RFI has a kurtosis that is different from that of Gaussian noise, the pulse detection algorithm assumes that the RFI is localized

in time and has a large instantaneous amplitude, while the peak picking and spectral kurtosis algorithms search for sinusoidal interference of an unknown frequency.

The next section introduces the notation to be utilized and the signal models considered in the absence and presence of RFI. Section III then introduces the pulse detection algorithm and derives its expected performance. This process is repeated in Section IV for the peak picking detector, and the kurtosis and spectral kurtosis detectors are reviewed in Section V. Results comparing the tests are provided in Section VI, and properties of the pulse detection algorithm are further explored in Section VII. Final conclusions and recommendations are provided in Section VIII.

II. Notation and Signal Models

A. Definitions

Consider a random variable α. The probability density function (pdf) of this random variable is denoted as $f_\alpha(\alpha_0)$, and satisfies

$$\int_{-\infty}^{\infty} d\alpha_0 \; f_\alpha(\alpha_0) \;=\; 1 \tag{1}$$

$$F_\alpha(\alpha_0) = P(\alpha < \alpha_0) \;=\; \int_{-\infty}^{\alpha_0} d\alpha_0 \; f_\alpha(\alpha_0) \tag{2}$$

Equation (2) defines the cumulative distribution function (cdf) of α. The probability of exceeding the value α_0 is given by $Q_\alpha(\alpha_0) = 1 - F_\alpha(\alpha_0)$, called the right tail distribution function henceforth.

For a set of independent random variables (α_1, α_2, $\cdots$, α_N), define γ as the maximum of the set. The cdf of γ is

$$F_\gamma(\gamma_0) = F_{\alpha_1}(\gamma_0) F_{\alpha_2}(\gamma_0) \cdots F_{\alpha_N}(\gamma_0) \tag{3}$$

This property will be used extensively to analyze detector properties in what follows.

B. Measurement process

To improve sensitivity in microwave radiometry, it is generally desirable to integrate observed powers over time periods that are as large as possible. The radiometer's output datarate is reduced by recording only the mean power estimate following this integration period. However such an approach reduces the ability to detect small duty cycle pulsed interferers that are present only for a small fraction of the integration time. For this reason, two time scales are considered in what follows. The first consists of N samples, and represents the time scale on which the pulse detection algorithm is implemented as well as the time scale on which a fast Fourier transform (FFT) is computed in the peak picking and spectral kurtosis methods. In the latter case, a single datapoint in N sub-channels is obtained every N time samples (the FFT computations are not overlapped.)

The second time scale is defined as IN samples, and represents the radiometer integration period. Within such a period, I outputs of the pulse detection algorithm and I spectra for the peak picking and spectral kurtosis methods occur. For the pulse and peak picking methods, final detectors over this set of I outputs are defined based on taking the maximum detector statistic among the I outputs; this is equivalent to declaring detection in an IN sample integration period if detection was declared in any of the I frames of N samples. This approach is chosen to retain sensitivity to short duty cycle interference at the cost of increasing the detector's false alarm rate. The spectral kurtosis algorithm uses all I outputs to estimate the kurtosis in each sub-channel; a composite detector is then created based on the maximum kurtosis value in all sub-channels. The single channel kurtosis algorithm uses the entire IN sample integration period (as in [9]).

As an example, a digital radiometer system sampling observed fields every 16 nsec (the Nyquist sampling rate for a 31.25 MHz bandwidth) is considered in what follows. N is varied from 8 to 256 samples (0.128 to 4.096 μsec) in order to capture time scales ranging from shorter than to comparable to those of expected radar pulses. The integration period IN is taken as 32768 samples, so that the total radiometer integration period is 524.288 μsec. While this integration period is somewhat smaller than that of many operational radiometers, it is expected that future radiometer systems designed to incorporate RFI mitigation will utilize shorter integration periods [16]. In what follows, as N is varied, the number of frames I is adjusted so that the integration period remains fixed.

C. Signal model when RFI is absent

In the absence of RFI, the sampled received fields are assumed to be uncorrelated Gaussian random variables with zero mean and standard deviation σ. For convenience σ is set to unity in what follows, so that all linear and power quantities are in units of σ and σ^2, respectively. Following [15], measured fields in the absence of RFI are written as

$$\begin{aligned} x_i[n] = w_i[n] \quad & n = 0, 1, \cdots, N-1 \\ & i = 0, 1, \cdots, I-1 \end{aligned} \tag{4}$$

where $w_i[n]$ refers to the independent identically distributed (i.i.d.) Gaussian measurements, and the separation of the integration period into I sets of N samples is apparent in the notation.

For this model, the square of a single field sample (i.e. proportional to the power) is a chi-squared random variable with one degree of freedom. If the field is squared and then summed over N samples, the sum X is a chi-squared random variable with N degrees of freedom. Following [15], the probability that such a random variable exceeds the value X_0 is denoted as $Q_{\chi^2_N}(X_0)$. The power estimate output by a microwave radiometer following an integration over N samples follows this distribution, and approaches a Gaussian distribution as N becomes large.

The pulse and peak picking detection algorithms to be considered require knowledge of the standard deviation σ of the RFI-free noise in order to set a relationship between the false alarm rate and the threshold used in the detection algorithm. In microwave radiometry, this standard deviation is proportional to the sum of the internal and external thermal noise power observed by the radiometer, which can vary with time. However, these time variations occur on time scales that

are large compared to those used in the detection algorithms to be described. The analyses that follow assume that a system exists for estimating the standard deviation of the RFI free noise on short time scales, and that the impact of errors in this estimate can be neglected. A system for obtaining this estimate through use of a "smart" averaging filter is described in [4]. Monte Carlo tests of the pulse and peak picking detectors using σ values estimated by a "smart" averaging filter having a 131 μsec time constant showed only slight differences from those to be reported in Sections VI and VII, with these differences reducing as the time constant of the averaging filter is increased. Therefore the remainder of the paper will neglect the impact of any imperfect estimation of the standard deviation of the RFI free noise.

D. Signal model when pulsed sinusoidal RFI is present

Reference [15] models received field samples when pulsed sinusoidal RFI is present for $i = 0, 1, \cdots, I-1$ as:

$$x_i[n] = \begin{cases} w_i[n] & n = 0, 1, \cdots, N-1 \\ & i \neq i_0 \\ A\cos(2\pi f_0 n + \phi) + w_i[n] & n = 0, 1, \cdots, N-1 \\ & i = i_0 \end{cases} \tag{5}$$

where $w_i[n]$ again refers to i.i.d. Gaussian random variables with zero mean and standard deviation one. In this case, sinusoidal interference has been added to frame i_0 of the I frames of N samples. The sinusoidal interference has an unknown arrival frame i_0, amplitude A, frequency f_0, and phase ϕ. For multiple integration periods, Reference [15] assumes that i_0 (an integer) is equally likely to take the values 0 through $I-1$, that $f_0 = k_0/N$ with k_0 an integer 1 to $N/2-1$, and that ϕ is uniformly distributed from 0 to 2π. Detector performance is examined as a function of A in [15].

Reference [15] shows that the generalized likelihood ratio test for this signal model reduces to a test on the maximum power observed within I sets of N-point FFT operations on the data. This "peak picking" approach on the data spectrogram is described further in Section IV.

The model used in [15] is generalized in this paper by allowing the frequency f_0 to be distributed uniformly and continuously from 0 to $1/2$ (the Nyquist frequency), by allowing multiple pulses to occur within the IN sample integration period, by allowing pulses to have a length not equal to N samples, and by allowing pulses to arrive at an arbitrary sample within an N point frame. In this case, pulses within the integration period have additional parameters describing the arrival sample $0 \leq N_s \leq N-1$ within frame i_0 as well as the pulse length (N_p samples.) The revised signal model for pulses can be expressed as

$$A\cos(2\pi f_0\left[(i-i_0)N + n\right] + \phi) + w_i[n] \tag{6}$$

for n and i values such that the function

$$\mathcal{I}(n,i) = \begin{cases} 1 & i_0 N + N_s \leq iN + n < i_0 N + N_s + N_p \\ 0 & \text{otherwise} \end{cases} \tag{7}$$

is non-zero.

When multiple pulses occur within an integration period the arrival frames (i indices i_0, i_1, $\cdots$) are drawn from the set $i = 0, \cdots, I-1$ so that no frame contains contributions from more than one pulse. This does not present difficulties for the low duty cycle interference of interest here, and none of the detection algorithms considered are sensitive to particular choices of the arrival frames. It is assumed for convenience that multiple pulses within the IN sized sample have identical amplitudes A and durations N_p, but the frequency f_0, phase ϕ, and arrival sample N_s are chosen independently. These choices result in an effective RFI duty cycle, d, within an integration period of

$$d = \frac{N_{pulse} N_p}{IN} \tag{8}$$

Note the duty cycle is restricted by the fact that the number of pulses in an integration period (N_{pulse}) is required to be an integer.

Sine wave amplitudes in what follows are described in terms of the ratio R of the average "signal-to-noise" power ratio ($dA^2/\left(2\sigma^2\right)$) normalized by the uncertainty in the radiometer power estimate ($\sigma^2/\sqrt{NI}$). This definition gives

$$R = \frac{dA^2}{2}\sqrt{NI} \tag{9}$$

$$A = \sqrt{\frac{2R}{d\sqrt{NI}}} \tag{10}$$

For $NI = 32768$, the maximum instantaneous signal to noise ratio is

$$A^2/2 = (5.52 \times 10^{-3})R/d \tag{11}$$

The choice of R as the RFI strength parameter of interest is motivated by the fact that RFI contributions on the order of $\sigma^2/\sqrt{NI}$ are the most difficult to detect in traditional radiometry. Interference that produces large R ($>\approx 10$) can be readily detected through examination of integrated powers on the IN sample time scale. Detector performance for interference having $0.25 \leq R \leq 1.5$ is examined in what follows.

1) Random phase model of RFI: Reference [9] describes fields when pulsed sinusoidal RFI is present as uncorrelated Gaussian random variables with zero mean and standard deviation σ plus sinusoidal RFI with a specified amplitude and a uniformly distributed random phase (as in [17]). In this model, RFI-containing datapoints are equally likely to occur anywhere within the size IN integration period (i.e. they do not necessarily occur successively in time) and all RFI-containing samples are independent of each other (i.e. no correlations in time.) This signal model appears acceptable for describing properties of the single channel kurtosis statistic (which does not utilize any information on the ordering of a data sample), and Monte Carlo comparisons of single channel kurtosis detector performance under the generalized model of Equations (5)-(6) and as predicted by the random phase model showed negligible differences for the cases considered in Section VI. However the random phase model is not applicable for describing radar or other pulsed source transmissions in detection algorithms that utilize sequential properties of the

measured data. The generalized signal model of Equations (5)-(6) is therefore used in studies of the pulse, peak picking, and spectral kurtosis detectors.

III. Pulse detection algorithm

The pulse detection algorithm to be described is an adaptation of the energy detector defined in [15], which can be regarded as the generalized likelihood ratio test in cases where the interfering signal is assumed to be deterministic but completely unknown. The pulse detection algorithm functions first by squaring incoming field samples, then averaging the resulting power over N samples. A local detection is declared if the result exceeds a specified threshold. A final detection is declared for the set of IN samples if any of the I individual N point detectors have declared detection. This is equivalent to a single detection using the maximum over I frames of the N point averages. The $Q_{\chi^2_N}(X_0)$ distribution for the integrated power in an RFI-free N-sample frame can therefore be aggregated over I independent RFI-free frames to obtain

$$Q_{pulse}^{noRFI}(X_0) = 1 - (1 - Q_{\chi^2_N}(X_0))^I \tag{12}$$

which provides the relationship between a threshold on RFI-free integrated power (X_0) and the false alarm rate of the pulse detection algorithm. For small false alarm rates, the false alarm rate is approximately linearly proportional to I.

When pulsed sinusoidal interference is present, frames containing RFI have a power integrated over N samples that is a non-central chi-squared random variable. The non-centrality parameter is

$$\lambda = \sum_{n=n_1}^{n_2} A^2 \cos^2(2\pi f_0 n + \phi) \tag{13}$$

where the beginning and ending indices n_1 and n_2 depend on the RFI arrival time N_s as well as the particular frame that is being considered within the set of N_f frames comprising an RFI pulse. The right-tail cdf of a non-central chi squared random variable is denoted following [15] as $Q_{\chi^2_N(\lambda)}(X_0)$. While the sum in equation (13) can be computed analytically, the result remains dependent upon both ϕ and f_0 as well as n_1 and n_2.

Given a threshold X_0 (chosen to set the false alarm rate) and the λ parameter, the probability of detection for a particular RFI-containing N-sample frame can be determined. Furthermore, the cdf for the maximum N-sample integrated power among the set of N_f frames containing a single RFI pulse can be determined using equation (3) if the λ values for each frame are known. This set of λ values is determined by the A, f_0, ϕ, N_s, and N_p parameters of the RFI pulse. The cdf for the maximum N-sample integrated power across N_{pulse} independent pulses can be obtained similarly as a product of the result for each individual pulse, as a function of the parameters for each of the pulses, of which f_0, ϕ, and N_s are assumed independent. The cdf for the maximum N-sample integrated power over an IN sample integration period also follows as the product of the cdfs for each of the individual pulses with the cdf for each of the remaining RFI-free frames (i.e. a central chi-squared random variable with N degrees of freedom). In this manner the probability of detection for the IN sample integration period is determined as one minus the final cdf given the A, f_0, ϕ, N_s, and N_p parameters for each of the N_{pulse} pulses.

A mean probability of detection for the entire integration period is then computed by numerically averaging the final product of $Q_{\chi^2_N(\lambda)}(X_0)$ and $Q_{\chi^2_N}(X_0)$ random variables over sets of λ values corresponding to f_0 uniformly distributed from 0 to $1/2$, ϕ uniformly distributed from 0 to 2π, N_s equally likely to take on the values 0 to $N-1$, and independent pulse parameters. The independence of multiple pulses within the integration period results in the averages being identical for each of the N_{pulse} pulses. The averaged right tail cdf is denoted by $Q_{pulse}(X_0)$; the numerical evaluation of a sum of double integrals is required for the determination of $Q_{pulse}(X_0)$. Numerical computations can be made reasonably efficient by first creating a table of the $Q_{\chi^2_N(\lambda)}(X_0)$ function in λ for each X_0 (i.e. false alarm rate) of interest; a routine in the DCDFLIB package [18] was used for evaluation of $Q_{\chi^2_N(\lambda)}(X_0)$.

IV. Spectrogram "peak picking"

Reference [15] shows that the generalized likelihood ratio test for the signal model of Equation (5) involves "peak picking" a spectrogram computed from the data, and describes a practical implementation based on the power in the subchannels of an N-point Fast Fourier Transform of each N-sample frame. A set of I of these spectra results for the IN sample integration period. The detector statistic T is implemented as

$$T = \max_{i,k} \frac{2}{N} \left| \sum_{n=0}^{N-1} x_i[n] \exp\left(-j2\pi \frac{k}{N} n\right) \right|^2 \tag{14}$$

with the maximum taken over the I spectra and the $N/2-1$ FFT channels indexed by $k = 1$ to $N/2-1$; the total number of FFT powers searched is then $L = I(N/2-1)$. For convenience in the following analysis, the $k=0$ and $k=N/2$ bins are omitted when computing the maximum due to the difference in properties between these bins (which contain purely real numbers) and those having $k=1$ to $N/2-1$.

The use of the FFT implies that this detector is explicitly searching for sinusoidal interference; the reliance on FFT powers results from the fact that the interference phase is unknown. The search over the set of FFT channels k and individual spectra i results due to the assumed unknown frequency and time of arrival of the sinusoidal interference. This detector essentially is a "max-hold" operation over measured spectra, followed by computation of the maximum power across frequency.

Reference [15] shows that the right tail distribution for T when RFI is absent is given by

$$Q_{peak}^{noRFI}(X_0) = 1 - (1 - Q_{\chi^2_2}(2X_0))^L \tag{15}$$

which establishes the false alarm behavior of the detector. It is shown in [15] that, for small false alarm rates, the false alarm rate is approximately linearly proportional to L.

The detector T is the generalized likelihood ratio test only for the specific signal model utilized by [15], which includes

the assumptions that the sinusoidal RFI frequency is $f_0 = \frac{k_0}{N}$ where k_0 is an integer from 1 to $N/2-1$, that the RFI pulse is exactly N samples, that the RFI pulse arrives always on the first sample of an N point frame, and that only a single RFI pulse is present within the IN size sample. Here the performance of the "peak picking" test is examined when these assumptions are removed.

First, for sinusoidal interference of arbitrary A, f_0, and ϕ occurring from samples n_1 to n_2 in an N-point frame, the result of the FFT operation can be expressed analytically (details not shown), and the power in each FFT channel k written as $\lambda_k(A, f_0, \phi, n_1, n_2)$. Reference [15] shows that in the presence of additive white Gaussian noise, the power in each of the FFT output channels $k = 1$ through $k = N/2-1$ is a non-central chi-squared random variable with two degrees of freedom and non-centrality parameter $\lambda_k(A, f_0, \phi, n_1, n_2)$. The cdf of the maximum power in channels $k = 1$ to $N/2-1$ is then

$$F_{peak}^{RFIframe}(X_0, A, f_0, \phi, n_1, n_2) = \prod_{k=1}^{N/2-1} (1 - Q_{\chi_2^2(\lambda_k(A,f_0,\phi,n_1,n_2))}(2X_0)) \quad (16)$$

Using equation (3), this result can then be aggregated with the N_f frames of an individual RFI pulse as well as N_{pulse} independent pulses and the remaining RFI-free frames to obtain the cdf for the maximum over i and k as a function of A, frequencies f_0, phases ϕ, and arrival times N_s of the independent pulses. The corresponding probability of detection is then numerically averaged over these parameters as for the pulse detection algorithm.

The use of an FFT algorithm in the peak-picking detector implies that sub-channel power information is available within the radiometer. If average brightnesses in all sub-channels are recorded following an IN sample integration period, RFI mitigation becomes possible by removing corrupted sub-bands, as described in [5], at the expense of an increased radiometer datarate. However such applications are not considered here due to the current focus on the detection of RFI in any portion of the radiometer observation.

V. Kurtosis and Spectral Kurtosis

The single channel kurtosis estimate is computed using the entire NI sample integration period, as in [9]. In the large sample limit, the kurtosis estimate approaches a Gaussian random variable with a known mean and variance. Monte Carlo tests using the generalized signal model described in Section II-D confirmed that the Gaussian approximation was acceptable for the 32768 sample integration period used here.

The spectral kurtosis method was implemented following [14] on powers output from an N point FFT operation. Given the powers in each FFT channel $k = 1$ to $N/2-1$, the spectral kurtosis in a given channel is proportional to the average of the power squared divided by the square of the average power, with the averages taken over the I spectra obtained in the integration period. The final spectral kurtosis detector is implemented by taking the maximum value of the kurtosis across channels $k = 1$ to $N/2-1$. Because kurtosis estimates are computed using a relatively small number of samples, it is difficult to predict their statistical properties. Monte Carlo simulations using 16384 realizations and the generalized signal model of Section II-D are relied upon exclusively in examining spectral kurtosis detector performance.

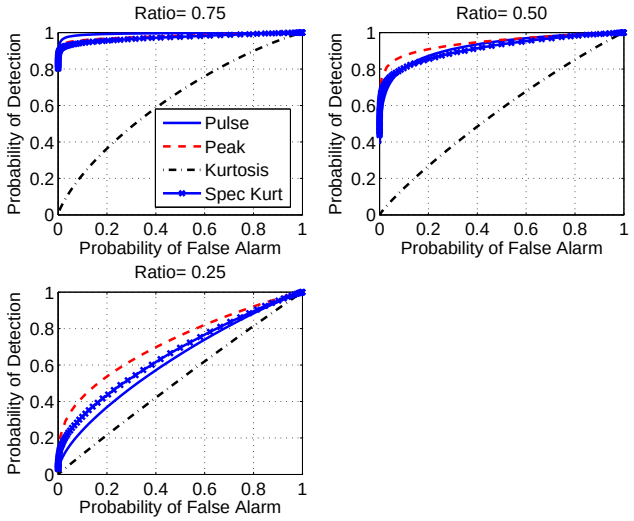

Fig. 1. Comparison of receiver operating characteristics for the pulse, peak-picking, single channel kurtosis, and spectral kurtosis detectors, using $N_p = 64$, $N = 32$, $N_{pulse} = 1$ (duty cycle 0.195%), and for $R = 0.75$ (plot (a)), $R = 0.5$ (plot (b)), and $R = 0.25$ (plot (c))

VI. Results

Figure 1 compares receiver operating characteristic (ROC) curves (i.e. plots of the probability of detection versus the probability of false alarm) for the case $N = 32$, $N_p = 64$ (pulse length 1.024 μsec), $N_{pulse} = 1$ (duty cycle 0.195%) for $R = 0.75$ (plot (a)), $R = 0.5$ (plot (b)), and $R = 0.25$ (plot (c)). Curves for the pulse, peak-picking, single channel kurtosis, and spectral kurtosis algorithms are shown. Similar results are plotted in Figures 2 and 3 for $N = 8$ and $N = 256$, respectively. For these parameters, the maximum instantaneous signal to noise ratio (equation 11) ranges from -1.5 dB ($R = 0.25$) to 3.3 ($R = 0.75$) dB.

An examination of Figures 1-3 shows that the pulse, peak picking, and spectral kurtosis algorithms generally have similar levels of performance, all of which exceed that achieved by the single channel kurtosis detector (which is identical in Figures 1-3 since no dependence on N is involved.) Performance of the N dependent algorithms is best for $N = 32$, which is the closest of the N values considered to the pulse length $N_p = 64$. For $N = 8$, the pulse detector out performs the peak picking and spectral kurtosis methods, presumably due to the relatively low spectral resolution achieved in these algorithms with $N = 8$. The pulse detection algorithm also outperforms the other methods for the N values shown with $R = 0.75$.

Figures 4 and 5 present similar performance comparisons for $N_p = 512$, $N_{pulse} = 1$ (duty cycle 1.56%) and for $N = 32$ (Figure 4) and $N = 256$ (Figure 5). In this case, the

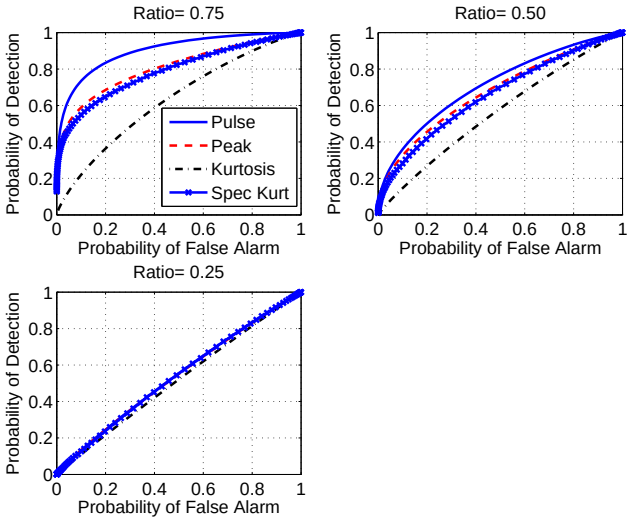

Fig. 2. Same as Figure 1 but for $N = 8$

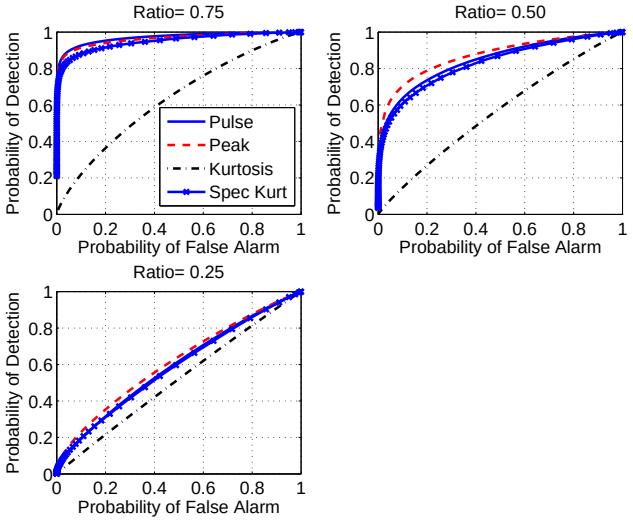

Fig. 3. Same as Figure 1 but for $N = 256$

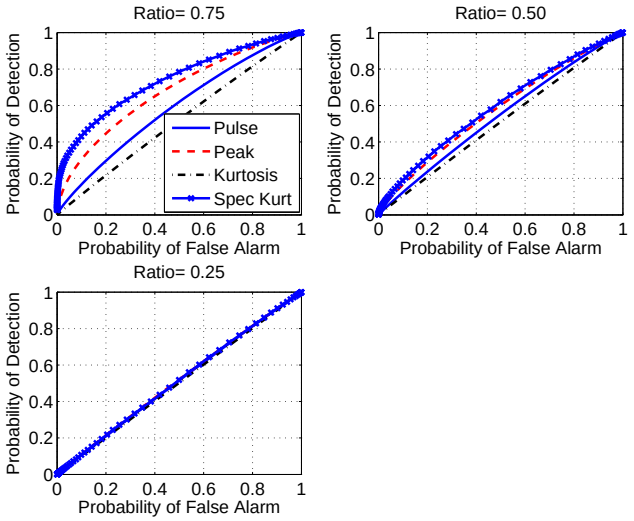

Fig. 4. Same as Figure 1 but for $N_p = 512$ and $N = 32$

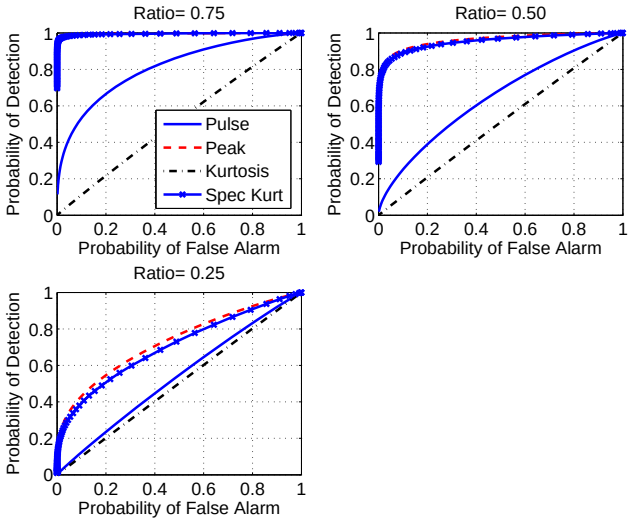

Fig. 5. Same as Figure 1 but for $N_p = 512$ and $N = 256$

greatly increased duty cycle results in a reduced RFI signal to noise ratio that ranges from -10.54 ($R = 0.25$) to -5.76 ($R = 0.75$) dB. Performance of the pulse detector is degraded due to the low instantaneous signal to noise ratios of the RFI, while the peak picking and spectral kurtosis methods show good performance for $N = 512$ due to the spectral resolution and associated processing gain from the correlation computed in each FFT bin. Results for $N = 32$ again show that performance degrades as the difference between N and N_p increases.

The influence of N is explored in detail for the peak picking and pulse detectors in Figures 6 ($N_p = 64$) and 7 ($N_p = 512$). Results in Figure 6 using $R = 0.5$ and $R = 1.5$ show a similar level of performance between the two detectors, and a strong impact of N in the $R = 0.5$ case, with the best detection performance achieved for $N = N_p = 64$. Pulse detector performance is less sensitive to N than that of the peak picking detector in the $R = 1.5$ case. Results in Figure 7 for $N_p = 512$ show similar trends with N as well as the degraded performance of the pulse detector at low R values for this larger duty cycle interference.

Overall these comparisons show that the pulse, peak picking, and spectral kurtosis algorithms have roughly similar performances for detecting pulsed sinusoidal interference in the cases considered, with all having increased sensitivity as the duty cycle of the interference is decreased (at a constant R value) and with all increasing in performance for N values near N_p. The pulse detection algorithm is the simplest of these three, since no FFT algorithm is required, but also suffers the largest decrease in performance as the interference duty cycle is increased. However, given the fact that many radar systems operate with duty cycles of 0.1% or less, the pulse detection algorithm appears to be well suited for detecting radar interference in microwave radiometry.

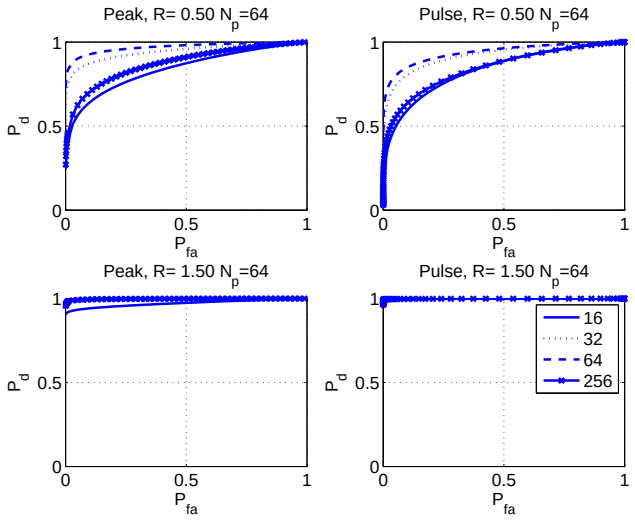

Fig. 6. ROC curves for the peak-picking (left) and pulse (right) detectors as N is varied for $N_p = 64$ and for $R = 0.5$ (top) and $R = 1.5$ (bottom)

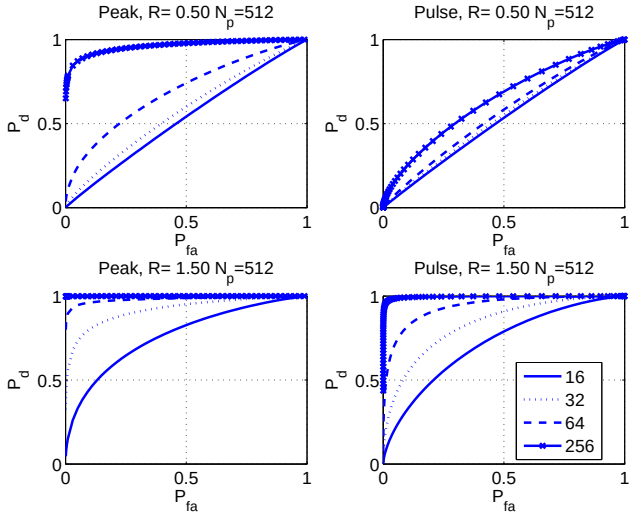

Fig. 7. Same as Figure 6 but for $N_p = 512$

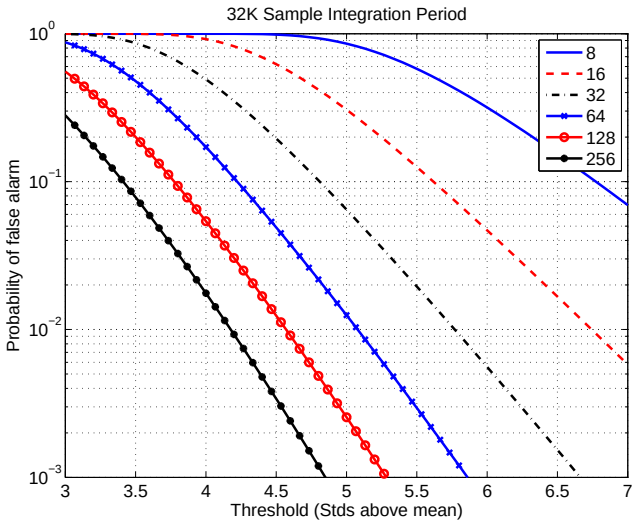

Fig. 8. False alarm rate for the pulse detection algorithm versus threshold, with N as a parameter and for a 32768 sample integration period. The horizontal axis value β is defined so that the threshold value is $N + \beta\sqrt{2N}$.

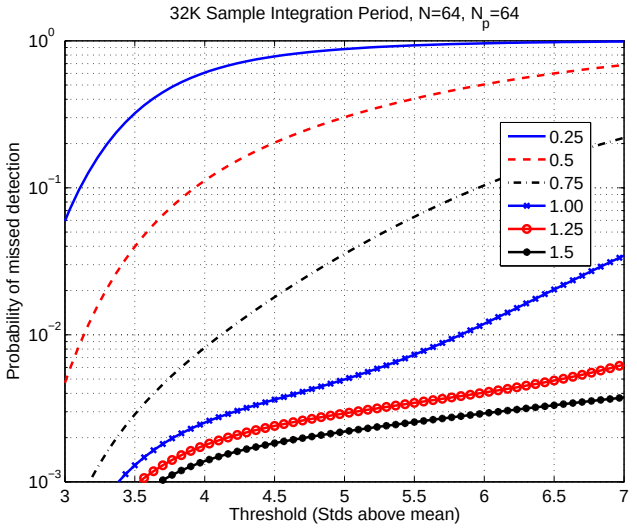

Fig. 9. Probability of a missed detection versus threshold with RFI strength R as a parameter, using $N = 64$, $N_p = 64$, and a 32768 sample integration period. The horizontal axis value β is defined so that the threshold value is $N + \beta\sqrt{2N}$.

VII. Further Analysis of Pulse Detection Algorithm

The simplicity of the pulse detection algorithm allows it to be incorporated as an "onboard" detector in a digital radiometer receiver, as in [5]. In this case, a fixed threshold value is used, and only the detection output (i.e. a single bit for each radiometer integration period) is recorded instead of the detector statistic itself. In such applications, properties of the detector as a function of the threshold level chosen are of interest. Here the threshold level is defined as a specified number of standard deviations of the N sample integrated power from its mean value, with both the mean and standard deviation computed in the absence of interference. For the chi-squared random variable with N degrees of freedom of the RFI-free pulse detection algorithm, the mean and standard deviation are N and $\sqrt{2N}$, respectively.

Figure 8 plots the false alarm rates achieved (equation (12)) versus this threshold for a 32768 sample integration period as N is varied. False alarm rates less than 1 percent are observed for $N = 32$ and $N = 64$ with thresholds of around 5.77 and 5.08 standard deviations above the mean, respectively.

Figure 9 plots the corresponding probability of a missed detection (i.e. one minus the probability of detection) versus threshold for multiple R values using a 32768 sample integration period, $N = 64$, and $N_p = 64$. At the one percent false alarm level (i.e. 5.08 on the horizontal axis) the probability of a missed detection is less than 4 percent for $R = 0.75$, and is less than 0.5 percent for $R = 1$.

Figure 10 plots the probability of a missed detection versus pulse length (assuming time samples at 16 nsec, so that the pulse length in microseconds is $0.016N_p$) for a 32768 sample integration period and for a fixed one percent probability of

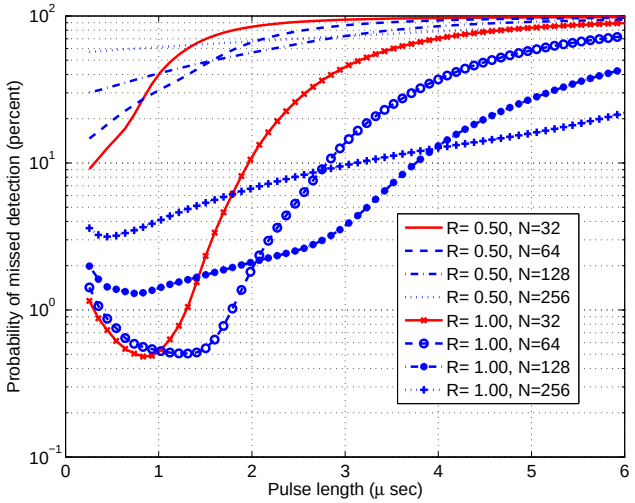

Fig. 10. Probability of a missed detection versus pulse duration in microseconds ($0.016N_p$) for a 1 percent probability of false alarm, with N and R as parameters as indicated in the legend.

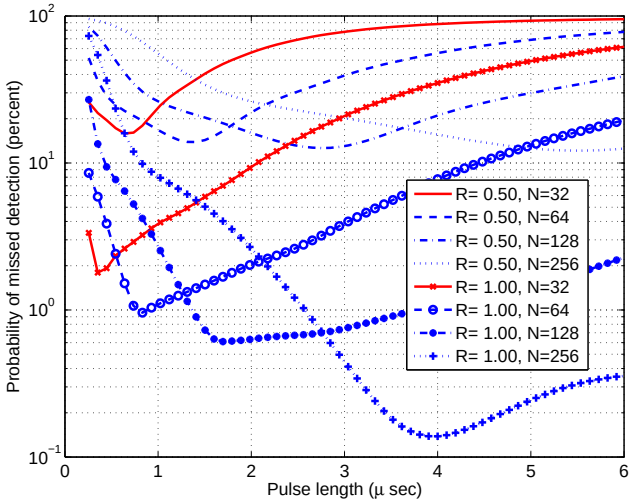

Fig. 11. Probability of a missed detection using the peak picking detector versus pulse duration in microseconds ($0.016N_p$) for a 1 percent probability of false alarm, with N and R as parameters as indicated in the legend.

false alarm. Probabilities of a missed detection in this case are greater than 9 percent for all the considered values of N for RFI strength $R = 0.5$. For $R = 1$, probabilities of missed detections of less than 0.5 percent are achieved with $N = 32$ and $N = 64$ for shorter pulse lengths (corresponding to lower duty cycles and higher instantaneous signal to noise ratios.) For fixed N and R, detection performance degrades as the pulse length exceeds N.

Figure 11 presents the same results as in Figure 10 for the peak picking detector. Performance is improved at $R = 0.5$ compared to the pulse detector for all but the shortest pulse lengths, although probabilities of missed detections remain greater than 10 percent. However the pulse detector with $N = 64$ yields better performance at $R = 1$ for pulse lengths less than 1.6 μsec, and the two are comparable for pulse lengths between 1.6 and 2 μsec. For larger pulse lengths, the peak picking detector with large N yields greatly improved performance due to its high spectral resolution and processing gain.

Figure 12 plots the probability of a missed detection for the pulse detection algorithm with $N = 64$ versus the RFI strength R, with N_p as a parameter. The false alarm rate is fixed at one percent as in Figures 10 and 11. Missed detection probabilities of less than one percent occur for all the considered N_p values at $R > 1.61$. The case $N_p = 64$ yields the best performance only for a limited range of R values, although it is competitive for the entire range. As expected, performance is observed to degrade as N_p becomes much larger or smaller than N.

As a final examination of the influence of the frame size N and pulse length N_p on the pulse detection and peak picking algorithms, Figure 13 provides contour plots of the probability of a missed detection for N and N_p varying over the range $16, 18, \cdots, 256$ and for a one percent false alarm probability. To include a finer range of N values in the plot, the integration period IN was allowed to vary with N so that I remains an integer; the resulting integration period is 32768 samples plus or minus $N/2$ samples as necessary.

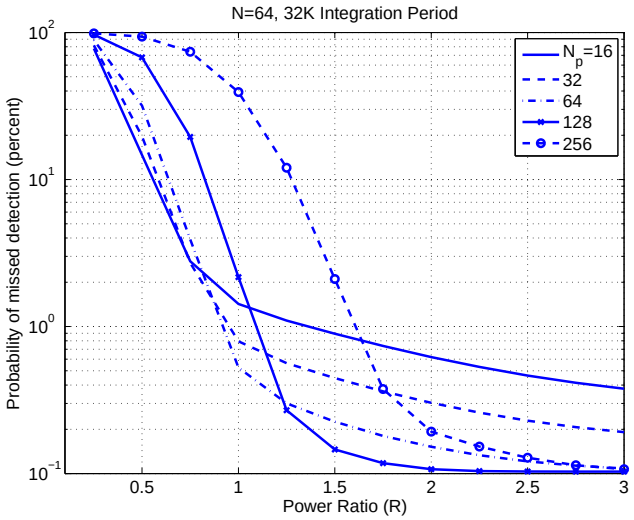

Fig. 12. Pulse detection algorithm probability of a missed detection versus RFI ratio R for a 1 percent probability of false alarm, with $N = 64$ and N_p as a parameter indicated in the legend.

The results show that the effect of N on pulse detection algorithm performance depends on the RFI strength R, with a larger sensitivity to N observed in Figure 13 at $R = 1$. As in Figures 10 and 12, performance is observed to be improved at $R = 1$ for N near N_p, and for the smaller N_p values that result in higher instantaneous signal-to-noise ratios for fixed R. Pulse detection algorithm sensitivity to N is greatly decreased for $R = 1.5$. In contrast, the detection performance of the peak picking algorithm generally increases with N when $N < N_p$, and improved performance continues to be observed in some cases for $N > N_p$ at larger R values. Comparison of the two results shows the pulse detection algorithm is more sensitive at $R = 1$ and 1.5 for smaller N values.

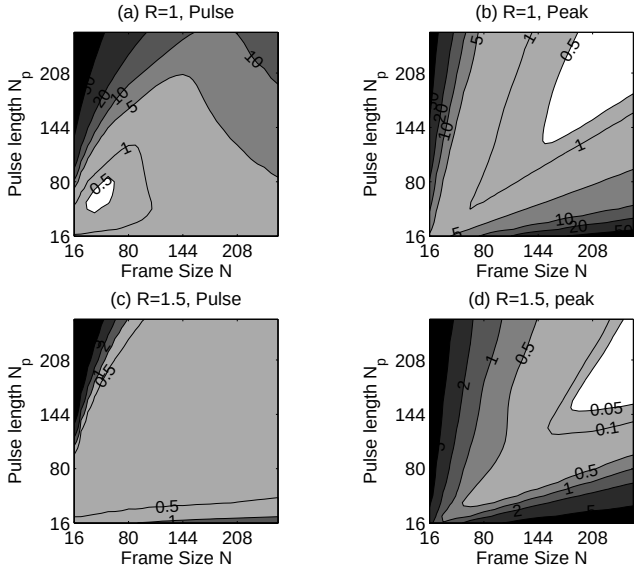

Fig. 13. Contour plots of pulse and peak picking algorithm probability of a missed detection (percent) versus N and N_p for a 1 percent probability of false alarm, with R as a parameter indicated in the plot titles.

VIII. Conclusions

The performance of four algorithms (the pulse, peak picking, single channel kurtosis, and spectral kurtosis methods) for detecting sinusoidal pulsed interference in microwave radiometer systems was compared. The RFI sources analyzed have an unknown frequency, initial phase, and time of arrival (which were averaged over in all the results shown) as well as an unknown duration and amplitude. Variations of detector performance with the latter two parameters as well as the detection algorithm internal time scale N were analyzed. Both the pulse and peak picking detectors have statistical properties that can be readily modeled, although numerical integrations are required in order to evaluate final detection probabilities.

Results show the pulse, peak picking, and spectral kurtosis algorithms to yield performance that is roughly comparable over the parameter space considered, while the single channel kurtosis detector was found to have less sensitivity than the other approaches. The pulse detection algorithm generally yielded excellent performance for pulsed interference with duty cycles of around 0.3 percent or less, but degraded as RFI duty cycles increased. All detectors showed improved performance when the internal time scale N was matched to the RFI pulse length. In general the exact pulse lengths of RFI sources are not known in microwave radiometry, but it can be expected that many radar interference sources will typically have pulse lengths of a few microseconds [13]. Use of $N \approx 64$ in the pulse detection algorithm seems reasonable based on these properties given the results in Figure 10.

While only pulsed sinusoidal RFI sources were considered here, it is to be expected that the pulse detector algorithm should remain effective against any impulsive RFI, regardless of source spectral properties, while the peak picking detector is matched to sinusoidal interference. Further analysis of combined detection and mitigation algorithms based on recording measurements in the multiple subchannels produced in the peak-picking and spectral kurtosis methods will be considered in future work.

References

[1] LeVine, D. M., "ESTAR experience with RFI at L-band and implications for future passive microwave remote sensing from space," *IEEE Geoscience and Remote Sensing Symposium,* conference proceedings, pp. 847–849, 2002.

[2] Camps, A., I. Corbella, F. Torres, J. Bara, and J. Capdevila, "RF interference analysis in aperture synthesis interferometric radiometers: application to L-band MIRAS instrument," *IEEE Trans. Geosc. Rem. Sens.,* vol. 38, pp. 942–950, 2000.

[3] G. A. Hampson, S. W. Ellingson, and J. T. Johnson, "Design and demonstration of an interference suppressing microwave radiometer," *IEEE Aerospace Conference,* conference proceedings, vol.2, pp. 993-999, 2004.

[4] N. Niamsuwan, J. T. Johnson, and S. W. Ellingson, "Examination of a simple pulse blanking technique for RFI mitigation" *Radio Science,* vol. 40, June 2005.

[5] B. Guner, J. T. Johnson, and N. Niamsuwan, "Time and frequency blanking for radio frequency interference mitigation in microwave radiometry," *IEEE Trans. Geosc. Rem. Sens.,* vol. 45, pp. 3672–3679, 2007.

[6] J. T. Johnson, A. J. Gasiewski, B. Güner, G. A. Hampson, S. W. Ellingson, R. Krishnamachari, N. Niamsuwan, E. McIntyre, M. Klein, and V. Y. Leuski, "Airborne radio-frequency interference studies at C-band using a digital receiver," *IEEE Trans. Geosc. Rem. Sens.,* vol. 44, pp. 1974-1985, 2006.

[7] A. J. Gasiewski, M. Klein, A. Yevgrafov, and V. Leuski, "Interference mitigation in passive microwave radiometry," *IEEE Geoscience and Remote Sensing Symposium,* conference proceedings, vol. 3, pp. 1682-1684, 2002.

[8] C. S. Ruf, S. M. Gross, and S. Misra, "RFI detection and mitigation for microwave radiometry with an agile digital detector," *IEEE Trans. Geosc. Rem. Sens.,* vol. 44, pp. 694-706, 2006.

[9] R. DeRoo, S. Misra, and C. Ruf, "Sensitivity of the kurtosis statistic as a detector of pulsed sinusoidal RFI," *IEEE Trans. Geosc. Rem. Sens.,* vol. 45, pp 1938–1946, 2007.

[10] S. Misra, S. S. Kristensen, S. S. Sojaerg, and N. Skou, "CoSMOS: Performance of Kurtosis Algorithm for Radio Frequency Interference Detection and Mitigation," Geoscience and Remote Sensing Symposium (IGARSS), conference proceedings, 2007.

[11] J. R. Piepmeier, P. Mohammed, and J. Knuble, "A Double Detector for RFI Mitigation in Microwave Radiometers," accepted by *IEEE Trans. Geosc. Rem. Sens.,* 2007.

[12] S. W. Ellingson and G. A. Hampson, "Mitigation of radar interference in L-band radio astronomy," *Astr. Journal Suppl, Ser.,* vol. 147, pp. 167–176, 2003.

[13] Ellingson, S. W. and M. Lewis, *Techniques for mitigation of radio frequency interference in radio astronomy,* Working document for ITU draft report, January 23rd, 2007 (available at `ftp://ftp2.naic.edu/pub/ast/murray/rfi/mitigation.pdf`).

[14] Nita, G., D. E. Gary, Z. Liu, G. Hurford, and S. M. White, "Radio frequency interference excision using spectral domain statistics," *Publ. Astron. Soc. Pacific,* vol. 119, pp. 805–827, 2007.

[15] S. M. Kay, *Fundamentals of Statistical Signal Processing: Volume II, Detection Theory,* Upper Saddle Creek, NJ: Prentice Hall, 1998.

[16] *Soil Moisture Active/Passive Mission Workshop Report,* available at `http://hydrology.jpl.nasa.gov/files/smap_11-01-07.pdf`, 2007.

[17] S. O. Rice, "Statistical properties of a sine wave plus random noise," *Bell Sys. Tech. Journal,* vol. 27, pp. 109–157, 1948.

[18] *DCDFLIB Package for computing cumulative distribution functions,* B. W. Brown, J. Lovato, and K. Russell, available at `http://www.netlib.org/random/`, 2007.